Spatiotemporal imaging of plasmonic fields near nanoparticles below the diffraction limit

Erfan Saydanzad, Jianxiong Li, and Uwe Thumm

Phys. Rev. A **98**, 063422 — Published 19 December 2018

DOI: 10.1103/PhysRevA.98.063422

Spatiotemporal imaging of plasmonic fields near nanoparticles below the diffraction limit

Erfan Saydanzad, Jianxiong Li, and Uwe Thumm
Department of Physics, Kansas State University, Manhattan,Kansas 66506, USA
(Dated: November 12, 2018)

Optically induced collective conduction-electron oscillations can generate intense plasmonic fields near metallic nanoparticles. We suggest a method for reconstructing such nanoplasmonic fields with nm spatial and sub-fs temporal resolution from streaked photoemission spectra. Applying this imaging scheme to Au nanospheres, we demonstrate the accurate spatiotemporal reconstruction of the plasmonic near-field distribution in comparison with the directly calculated plasmonic field.

PACS numbers: 73.20.Mf, 78.20.Bh, 78.47.J-

I. INTRODUCTION

Metallic nanostructures may respond to incident visible or infrared (IR) light by generating strong induced electromagnetic fields. These nanoplasmonic fields can exhibit nm-scale variations and can exceed the incident-field intensity near nanostructured surfaces [1–6] and isolated nanoparticles [7, 8] by orders of magnitude [9]. The underlying extraordinarily strong polarizability is due to the high mobility of conduction electrons that are driven collectively and in phase (owing to the structures' sub-wavelength size) by the incident radiation. Controllable strong localized induced plasmonic fields near nanostructured surfaces and isolated plasmonic nanoparticles promise to increase the efficiency of existing and enable novel applications in nanoplasmonically enhanced photocatalysis [10], light harvesting [11], time-resolved nanoplasmonic-field microscopy [1], surface-enhanced Raman spectroscopy [12], biomedical and chemical sensing [13, 14], tumor detection and treatment [15, 16], femtosecond scanning tunneling microscopy and spectroscopy [17], and ultrafast electro-optical switching [18]. Progress in these promising applications will be facilitated and possibly depend on the accurate nm–sub-fs scale spatiotemporal characterization of transient nanoplasmonic fields, calling for the design of novel schemes for the reconstruction of plasmonic field distributions.

Laser technology has advanced to allow the interrogation of the electronic dynamics in gaseous atoms and molecules with a resolution in time of a few attoseconds (1 as $= 10^{-18}$ seconds), and attosecond science is rapidly expanding to time-resolved investigations of (collective) electronic processes in solid matter [18–20]. Attosecond streaked photoemission spectroscopy, in particular, by illuminating a target with isolated attosecond extreme ultraviolet (XUV) pulses that are phase-coherently synchronized to a delayed strong IR (or visible) pulse, records photoemission yields as a function of the delay τ between the ionizing XUV and assisting streaking pulses, revealing temporal information through relative phase shifts of delay-dependent photoelectron yields (so-called "streaking traces") from different initial electronic states of the target [20, 21]. In streaked photoelectron spectra of nanoparticles [8, 22–24] and nanotips [25, 26], the nanoplasmonic response to the streaking pulse leads to a characteristic amplitude increase and phase shift of the streaking traces, providing temporal information on the induced plasmon-dynamics.

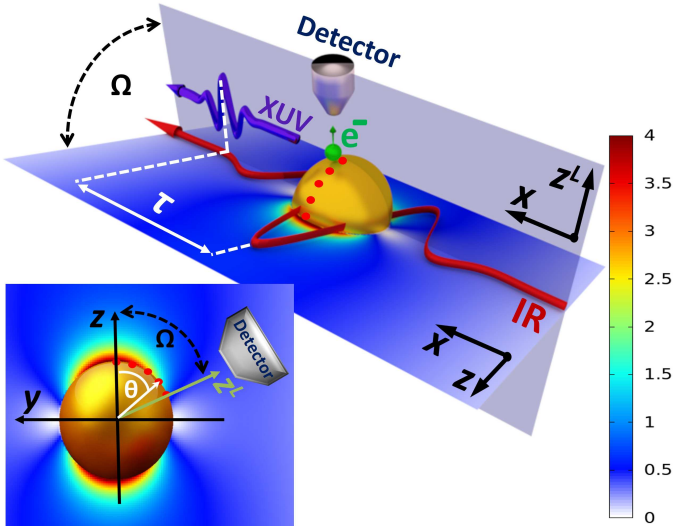

Figure 1. (Color online) Spatiotemporal nanoplasmonic field imaging near isolated metallic nanospheres employing streaked photoemission spectroscopy. Electrons released by isolated XUV pulses are streaked by delayed nanoplasmonically enhanced visible or IR pulses upon leaving the particles' surface. τ designates the time delay between the phase-coherent streaking and XUV pulses, Ω the variable angle between the XUV and IR electric-field linear polarization directions. Red dots indicate points on the "$x = 0$ *longitude*".

While streaked photoemission from nm-sized metallic structures proceeds across the inhomogeneous plasmonic field, the spatiotemporal plasmonic field distribution has not yet been extracted from streaked spectra. In the present work both, the numerical modeling of streaked spectra and the reconstruction of plasmonic near-fields from simulated spectra are based on the classical representation of the photoelectron dynamics. This work is an

extension of our previous studies on photoemission from plasmonic targets [8, 22, 23], in which we investigated the retrieval of the temporal structure of plasmonic near fields from streaked photoemission spectra with sub-fs resolution in time. In the present work we (i) numerically investigate a novel imaging scheme that adds nm spatial resolution of the plasmonic near field, by means of a suggested modification of the default experimental set up for recording streaked photoelectron spectra [20], and (ii) give a detailed mathematically description of the underlying spatiotemporal reconstruction algorithm. The suggested plasmonic field-retrieval algorithm is applicable for sufficiently long streaking pulses, complementing a recently suggested quantum-mechanical field-retrieval scheme that was optimized for ultrashort IR streaking pulses [27].

The proposed scheme for retrieving the plasmonically enhanced streaking electric-field distribution near metal nanospheres with high spatiotemporal resolution consists in recording streaked spectra for variable relative linear polarization directions Ω of the attosecond XUV and streaking pulse (Fig. 1). We assume both pulses to propagate along the x-axis of the lab frame (x, y^L, z^L), which is centered in the nanosphere of radius a. The XUV pulse is polarized along the z^L-axis, and the streaking pulse along z-axis of the rotated (x, y, z) reference frame. A stream of isolated spherical gold nanoparticles is injected by aerodynamic lens focusing [28–31] into the laser-interaction region. The laser parameters assumed in our numerical examples correspond to typical parameters used in streaked photoemission experiments with gaseous and solid targets [7, 20, 21, 25, 28, 30]. We can safely neglect the thermal melting of the nanoparticles due to the applied external laser pulses. Melting eventually occurs, however, at a picosecond time scale and therefore long after the few femtoseconds an emitted photoelectron needs to traverse and "probe" the plasmonic near field. Recent experiments measured streaked photoelectron spectra from tapered Au nanowires with 0.1 TW/cm^2 NIR pulses [25] and estimated the damage threshold for Au nanowires at 10 TW/cm^2 for 32 fs pulses and 5 TW/cm^2 for 108 fs pulses [32].

We will show how variation of Ω allows the reconstruction of the total electric field distribution (sum of induced plasmonic and incident streaking field) (i) along the "$x = 0$ *longitude*" with rotated-frame coordinates $(a, \phi = -\pi/2, \theta = \Omega)$ (indicated as red dots in Fig. 1)) and (ii), in consequence, over the entire nanoparticle surface. Unless stated otherwise, we use atomic units ($\hbar = e = m_e = 1$). To conveniently keep track of relative phases, we employ complex-valued electric fields, their real parts representing physical fields.

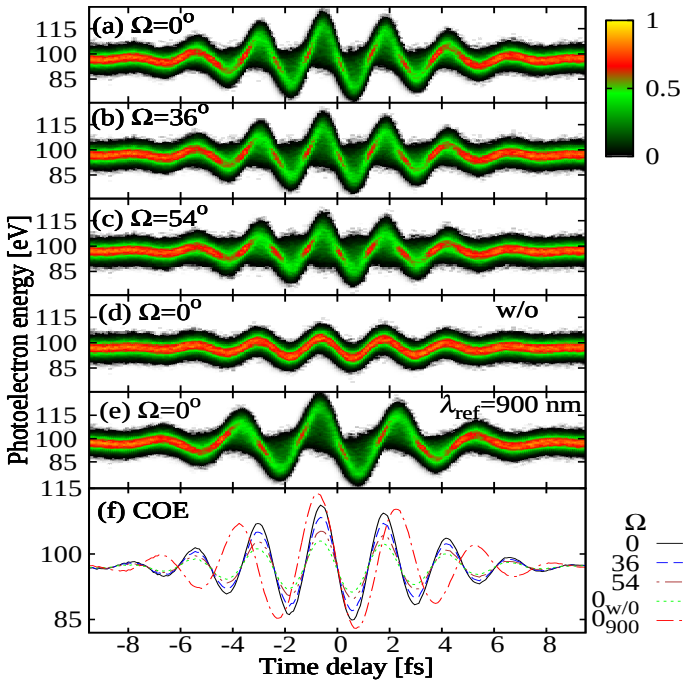

Figure 2. (Color online) Streaked spectra from 25 nm radius Au nanospheres for different polarization directions Ω and $\lambda = 720$ nm (a-c) with and (d) without including $\vec{E}_{pl}$. (e) Streaked reference spectrum for $\Omega = 0$ and $\lambda = 900$ nm including $\vec{E}_{pl}$. (f) Corresponding centers of energy.

II. SPATIOTEMPORAL ATTOSECOND STREAKING

We assume Gaussian XUV pulses with central energy $\varepsilon^{ctr}_{xuv} = 105$ eV and full temporal width at half intensity maximum (FWHIM) $\Delta t_{xuv} = 287$ as, given by the electric field

$$\vec{E}_{xuv}(\vec{r}, t) = E_{xuv,0} \exp\left[-2\ln 2 \frac{(t - x/c)^2}{\Delta t^2_{xuv}}\right] \times \exp\left[-i\varepsilon^{ctr}_{xuv}(t - x/c)\right] \hat{e}_{z^L} \quad (1)$$

and streaking pulses with Gaussian temporal profile

$$\vec{E}_{inc}(\vec{r}, t) = -E_{IR,0} \exp\left[-2\ln 2 \frac{(t + \tau - x/c)^2}{\Delta t^2_{IR}}\right] \times \exp\left[-i\omega(t + \tau - x/c)\right] \hat{e}_z \quad (2)$$

of pulse length (FWHIM) $\Delta t_{IR} = 5.9$ fs, $\lambda = 2\pi/k = 2\pi c/\omega$ central wavelength, and 10^{12} W/cm^2 peak intensity. c designates the speed of light in vacuum, and the coordinate unit vectors are related as $\hat{e}_z = \sin\Omega\ \hat{e}_{y^L} + \cos\Omega\ \hat{e}_{z^L}$. The time delay τ between the XUV and the streaking pulses is defined to be positive if the streaking pulse precedes the XUV pulse.

The inhomogeneous induced plasmonic field near the surface of sub-streaking-pulse-wavelength-sized

nanospheres is given in dipole approximation by [33]

$$\vec{E}_{pl}(\vec{r},t) = p(t)\frac{e^{ikr}}{r^3}\left[3(1-ikr)-k^2r^2\right]\sin\theta\cos\theta\ \hat{e}_\rho + p(t)\frac{e^{ikr}}{r^3}\left[k^2r^2\sin^2\theta+(1-ikr)(3\cos^2\theta-1)\right]\ \hat{e}_z, \tag{3}$$

where $\hat{e}_\rho$ and $\hat{e}_z$ are unit vectors in cylindrical coordinates. We used the expression for the oscillating induced dipole moment $p(t)$ calculated within Mie theory [34] as given in Ref. [35], such that (3) is valid for size parameters $2\pi a/\lambda <\approx 0.6$ [22]. The strength of the total electric field near the nanosphere, $\vec{E}_{tot} = \vec{E}_{inc} + \vec{E}_{pl}$, on the nanosphere surface at time $t = 0$ is

$$E_{tot}(a,\phi,\theta,\tau) = \eta_\lambda(a,\theta)E_{inc}(a,\phi,\theta,t=0) \times \exp\left\{-i\left[\sigma_\lambda(a,\theta)+\pi\right]\right\}. \tag{4}$$

While E_{tot} does not have cylindrical symmetry, due to the dependence of $x = x_s = a\sin\theta\cos\phi$ in E_{inc} on ϕ, the plasmonic-field enhancement $\eta_\lambda(a,\theta)$ and phase shift $\sigma_\lambda(a,\theta)$ are cylindrically symmetrical [cf., Eq. (3)]. According to Eq. (4), retrieval of $E_{tot}(a,\phi,\theta,\tau)$ along the $x = 0$ *longitude* therefore allows the reconstruction of the electric-field distribution on the entire nanoparticle surface. In slowly-varying-amplitude approximation, the vector potential of the incident and total electric field follow from (2) and (4) as

$$A_{inc}(a,\phi,\theta,\tau) \simeq \frac{-i}{\omega}E_{inc}(a,\phi,\theta,t=0) \tag{5}$$

and

$$A_{tot}(a,\phi,\theta,\tau) = \eta_\lambda(a,\theta)A_{inc}(a,\phi,\theta,\tau) \times \exp\left[i\sigma_\lambda(a,\theta)\right]. \tag{6}$$

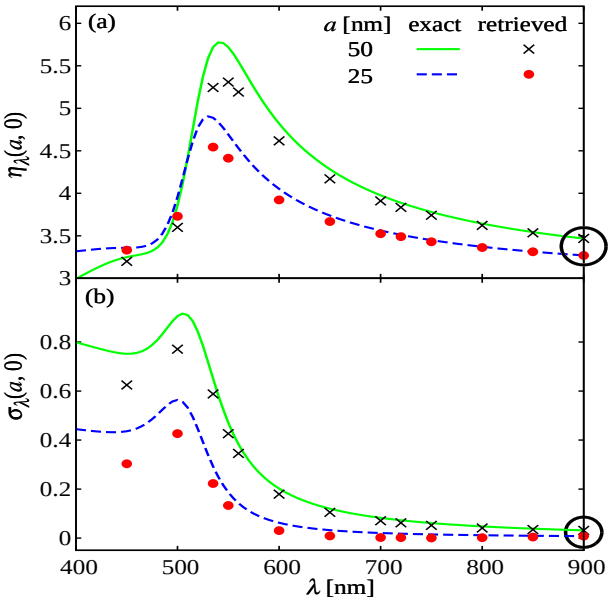

Figure 3. (Color online) Plasmonic (a) field enhancements and (b) phase shifts at the pole ($\theta = 0$) of gold nanospheres with radii of 25 and 50 nm as a function of the incident streaking-field wavelength λ. The peak intensity of the streaking field is 10^{12} W/cm^2. Exact results (solid and dashed lines) are calculated based on classical electrodynamics according to Eqs. (3) and (4). Symbols show values retrieved from simulated streaked photoelectron spectra. Values at the reference wavelength of 900 nm used for the plasmonic-field retrieval are circled.

We calculated streaked spectra within a classical trajectory model, modeling photoemission in four distinct steps: (i) electronic excitation by the XUV pulse followed by electron (ii) transport to the surface, (iii) escape from the surface, and (iv) propagation outside the nanosphere under the influence of $\vec{E}_{tot}$. The spectra were assembled based on a phenomenological probability distribution over at least six million phase-space points that serve as initial values for Monte-Carlo sampled trajectories. A detailed description of this approach is given in Ref. [22]. We numerically simulated streaked spectra for a streaking wavelength of $\lambda = 720$ nm and 10 relative polarizations $0 \le \Omega \le \pi/2$. Figures 2(a)-2(c) show spectra for $\Omega = 0, 36$ and $54°$ from 25 nm radius nanospheres. A spectrum for $\lambda = 720$ nm without including the plasmonic field is given in Fig. 2(d) for $\Omega = 0$. The spectrum for $\lambda = 900$ nm and $\Omega = 0$ is taken as the reference for the plasmonic field retrieval [Fig. 2(e)]. The center of energies (COEs) of the spectra in Figs. 2(a)-2(e) are the first moments of the energy distributions in the energy interval [70, 130] eV [Fig. 2(f)]. Fitting these numerically calculated COEs to the function

$$\varepsilon^j_\lambda(a,\phi,\Omega,\tau) = \varepsilon_0 + C^j_\lambda(a,\Omega)\exp\left[-2\ln 2\frac{(\tau-x_s/c)^2}{\Delta t^2_{IR}}\right] \times \exp\left\{-i\left[\omega(\tau-x_s/c)+\beta^j_\lambda(a,\Omega)\right]\right\} \tag{7}$$

yields the peak COE amplitude $C^j_\lambda(a,\Omega)$ and COE phase shift $\beta^j_\lambda(a,\Omega)$. The COEs oscillate about the unstreaked central photon energy $\varepsilon_0 = \varepsilon^{ctr}_{xuv} - W - 2\varepsilon_f/5$, where $W = 5.1$ eV is the work function and $\varepsilon_f = 5.5$ eV the Fermi energy for bulk gold [22]. The superscript $j = w, w/o$ indicates calculations with/without $\vec{E}_{pl}$.

The simulation of streaked photoemission from atoms in strong-field approximation results in streaking amplitudes $\varepsilon^j_\lambda(a,\phi,\Omega,\tau) - \varepsilon_0$ proportional to $A_{inc}(a,\phi,0,\tau)$ [20]. Guided by this well-know proportionality, we base the plasmonic field reconstruction on the heuristic expression

$$\frac{A_{tot}(a,\phi,\Omega,\tau)}{A_{inc}(a,\phi,0,\tau)} = \frac{\varepsilon^w_\lambda(a,\phi,\Omega,\tau) - \varepsilon_0}{\varepsilon^{w/o}_\lambda(a,\phi,0,\tau) - \varepsilon_0} \times \alpha(a)\exp\left[i\psi(a)\right], \tag{8}$$

introducing the factor $\alpha(a)$ to correct the attenuation of the plasmonic COE amplitude enhancement $C^w_\lambda(a,\Omega)/C^{w/o}_\lambda(a,0)$ relative to the plasmonic electric field enhancement. This COE enhancement correction accounts for (i) the streaking trace including contributions from photoelectrons emitted over *entire* surface, thus including regions where the vector potential is significantly differs from $A_{tot/inc}(a,\phi,\Omega,\tau)$, and (ii) the propagation of photoelectrons in the inhomogeneous plasmonic field resulting in their exposure to an effective electric field that is weaker than the electric field at the surface. Similarly, we allow for a cumulative phase shift $\psi(a)$ in order to represent (i) the spectral averaging inherent in the calculation of COEs, (ii) scattering of photoelectrons during their transport to the surface (step two in our photoemission model [22]), (iii) electron escape from the surface (step three), and (iv) subsequent photoelectron propagation in the inhomogeneous plasmonic field (step four). Dividing (6) by (5) and (7) with $j = w$ by (7) with $j = w/o$ we obtain

$$\eta_\lambda(a,\Omega) = \frac{C^w_\lambda(a,\Omega)}{C^{w/o}_\lambda(a,0)}\alpha(a) \tag{9}$$
$$\sigma_\lambda(a,\Omega) = \beta^{w/o}_\lambda(a,0) - \beta^w_\lambda(a,\Omega) + \psi(a).$$

Justified by our numerical results shown below, we neglect the dependence of $\alpha(a)$ and $\psi(a)$ on the streaking wavelength and Ω. Therefore, comparison with a reference streaking spectrum taken for a streaking wavelength where the plasmonic response is either weak or can be neglected, e.g. $\lambda_{ref} = 900$ nm with polarization direction $\Omega = 0$ [cf., Figs. 3 and 2(e)], allows us to eliminate the factors $\alpha(a)$ and $\psi(a)$ in (9). In this work, we assume $\lambda_{ref} = 900$ nm and $\Omega = 0$ for the reference spectrum. The plasmonic-field enhancement and phase shift for the wavelength λ of interest can now be retrieved from streaked spectra as expressed in

$$\eta_\lambda(a,\Omega) \simeq \overbrace{\eta_{\lambda_{ref}}(a,0)}^{a:\ ED-theory} \times \overbrace{\left[\frac{C^{w/o}_{\lambda_{ref}}(a,0)}{C^{w/o}_\lambda(a,0)}\right]}^{b:\ Simulation} \times \overbrace{\left[\frac{C^w_\lambda(a,\Omega)}{C^w_{\lambda_{ref}}(a,0)}\right]}^{c:\ Experiment} \tag{10}$$

$$\sigma_\lambda(a,\Omega) \simeq \overbrace{\sigma_{\lambda_{ref}}(a,0)}^{a:\ ED-theory} + \overbrace{\left[\beta^{w/o}_\lambda(a,0) - \beta^{w/o}_{\lambda_{ref}}(a,0)\right]}^{b:\ Simulation} + \overbrace{\left[\beta^w_{\lambda_{ref}}(a,0) - \beta^w_\lambda(a,\Omega)\right]}^{c:\ Experiment}.$$

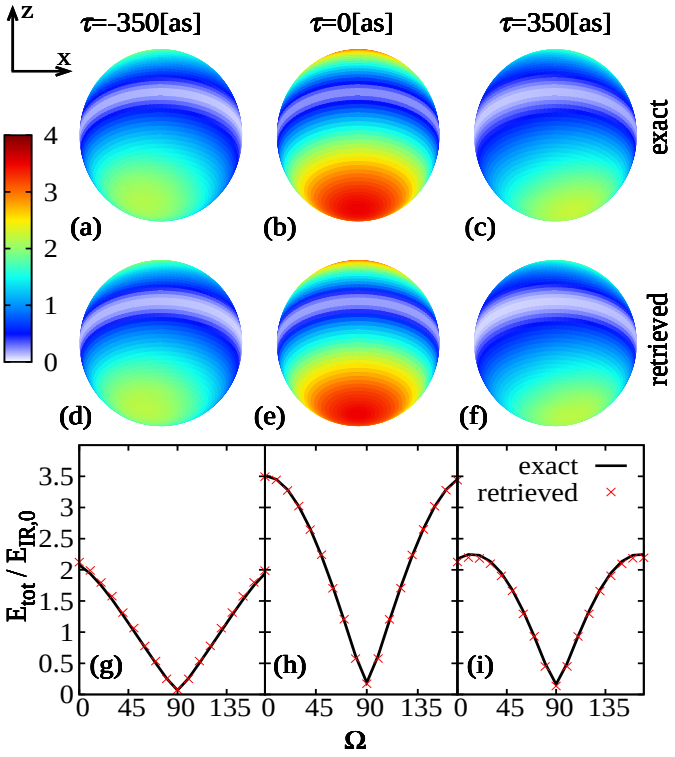

Figure 4. (Color online) Results for 25 nm Au nanospheres for three XUV-IR pulse delays τ. (a-c) Calculated exact and (d-f) retrieved total electric fields at the surface, normalized to the IR-laser-pulse amplitude $E_{IR,0}$.(g-i) Exact and retrieved total electric field versus the polar angle $\theta = \Omega$ along the *x=0 longitude* ($\phi = 0$).

The retrieval process thus has three three distinct parts as indicated in the annotations of the above equation:

a: The plasmonic enhancement and phase shift at the reference wavelength are calculated within classical electrodynamics (ED) [22, 34]. $\sigma_{\lambda_{ref}}(a,0)$ may be negligible (cf. Fig. 3).

b: Not accessible experimentally, the COEs $C^{w/o}_{\lambda_{ref}}(a,0)$ and $C^{w/o}_\lambda(a,0)$ and phase shifts $\beta^{w/o}_\lambda(a,0)$ and $\beta^{w/o}_{\lambda_{ref}}(a,0)$

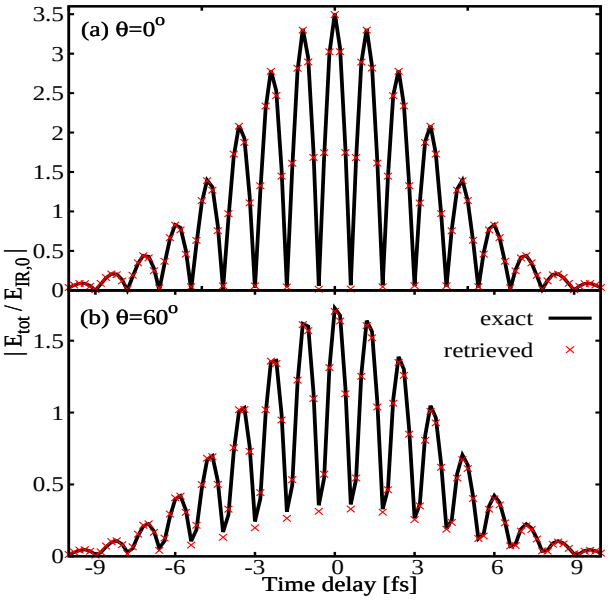

Figure 5. (Color online) Exact and retrieved total electric near field, normalized to the IR-laser-pulse amplitude $E_{IR,0}$, versus the XUV-IR pulse delays τ for 25 nm Au nanospheres for two different polar angles.

neglecting the plasmonic response are derived from simulated spectra. Our numerical results show that these functions are size-independent for radii $a \in [5,\ 50]$ nm and only depend on the incident streaking-pulse wavelength. To facilitate the field reconstruction at different streaking wavelength, we therefore provide linear fits, valid for the range $\lambda \in [400,\ 900]$ nm, of the response-free COEs and phase shifts, $C_\lambda^{w/o}(a,0) = \mu_1 + \mu_2\ \lambda$ and $\beta_\lambda^{w/o}(a,0) = \pi/2 + \kappa/\lambda$, with adjusted parameters $\mu_1 = -0.316, \mu_2 = 8.60\times10^{-3}$ nm^{-1}, and $\kappa = 87.82$ nm. **c:** These factors include COEs and phase shifts deduced from measured spectra at the streaking wavelengths λ and λ_{ref}. $C_\lambda^w(a,\Omega)$ and the phase shifts $\beta_\lambda^w(a,\Omega)$ are measured for several polarization directions Ω.

III. SPATIOTEMPORALLY-RESOLVED SURFACE-ELECTRIC-FIELD DISTRIBUTIONS

Figure 3 shows retrieved plasmonic-field enhancements $\eta_\lambda(a,0)$ and phase shifts $\sigma_\lambda(a,0)$ for 25 and 50 nm radius nanospheres for 400 nm $< \lambda <$ 900 nm in fair agreement with our classical ED calculations. Upon retrieving $\eta_\lambda(a,\theta=\Omega)$ and $\sigma_\lambda(a,\theta=\Omega)$ for 11 equally-spaced relative polarizations $\Omega = 0, 9°, 18°, ..., 90°$ from simulated spectra for 25 nm nanosphere radius and 720 nm streaking wavelength, we reconstructed the total electric fields at different delays at the nanoparticle surface according to Eq. (4) with nm spatial resolution. The retrieved and exact fields agree (Fig. 4).

The spatial resolution of the reconstructed plasmonic near field depends on the number of polarization directions Ω for which spectra are recorded. Based on $N_\Omega = 11$ equally spaced angles $0 \le \Omega \le 90°$, the present application of our imaging scheme results in a spatial resolution of the retrieved field of $(1/(N_\Omega - 1) * (\pi/2) * a \approx 4$ nm. The best achievable spatial resolution is limited since streaking traces produced by photoelectrons originating from very nearby points on the surface cannot be distinguished. Figure 5 shows excellent agreement between the exact and retrieved total electric fields as functions of the time delay τ for $\phi = 0°$ and two polar emission angles, $\theta = \Omega = 0°, 60°$.

IV. CONCLUSION

In summary, we propose a with current technology practicable spectroscopic scheme based on attosecond streaking spectroscopy which, by scanning the relative linear polarization direction of the XUV and streaking pulse, allows the imaging of plasmonic electric-field distributions on the surface of spherical nanoparticles with nm spatial and sub-fs temporal resolution. The implementation of this method requires the extension of conventional streaking measurements from nanoparticles by allowing for the controlled rotation of the relative linear polarization direction between the XUV and the IR pulses. The suggested imaging scheme has the potential to be generalized to non-spherical nanoparticles by enabling the rotation of the electron detector or by adding multiple detectors at different directions. For full spatial resolution of the electric near-field distribution, the extension to non-spherical particles may require alignment of the nanoparticles. Further improvements of the suggested imaging scheme may result in a powerful method for the scrutiny of nanoscopic plasmonically enhanced electric-field distributions and electronic dynamics on functional nanoparticles and nanostructured surfaces.

ACKNOWLEDGEMENTS

This work was primarily supported by the Air Force Office of Scientific Research award no. FA9550-17-1-0369 (Recollision physics at the nanoscale). Additional support through NSF grants no. PHY 1464417 and 1802085 (Theory for photoemission from surfaces), and the Chemical Sciences, Geosciences, and Biosciences Division, Office of Basic Energy Sciences, Office of Science, U.S. DOE under award no. DE-FG02-86ER13491 (Attosecond interferometry and photoemission from atoms in spatially varying external fields) is also gratefully acknowledged.

REFERENCES

[1] M. I. Stockman, M. F. Kling, U. Kleineberg, and F. Krausz, Nat. Photonics **1**, 539 (2007).

[2] A. Kinkhabwala, Z. Yu, S. Fan, Y. Avlasevich, K. Müllen, and W. Moerner, Nat. Photonics **3**, 654 (2009).

[3] S. L. Stebbings, F. Süßmann, Y. Y. Yang, A. Scrinzi, M. Durach, A. Rusina, M. I. Stockman, and M. F. Kling, New J. Phys. **13**, 073010 (2011).

[4] E. Skopalová, D. Lei, T. Witting, C. Arrell, F. Frank, Y. Sonnefraud, S. Maier, J. Tisch, and J. Marangos, New J. Phys. **13**, 083003 (2011).

[5] M. Becker, W. C.-W. Huang, H. Batelaan, E. J. Smythe, and F. Capasso, Ann. Phys. (Berlin) **525**, L6 (2013).

[6] P. Dombi, A. Horl, P. Racz, I. Marton, A. Trugler, J. R. Krenn, and U. Hohenester, Nano Lett. **13**, 674 (2013).

[7] S. Zherebtsov, T. Fennel, J. Plenge, E. Antonsson, I. Znakovskaya, A. Wirth, O. Herrwerth, F. Süßmann, C. Peltz, I. Ahmad, S. A. Trushin, V. Pervak, S. Karsch, M. J. J. Vrakking, B. Langer, C. Graf, M. I. Stockman, F. Krausz, E. Ruhl, and M. F. Kling, Nat. Phys. **7**, 656 (2011).

[8] J. Li, E. Saydanzad, and U. Thumm, Phys. Rev. A **94**, 051401 (2016).

[9] M. I. Stockman, Physics Today **64** (2011).

[10] A. E. Schlather, A. Manjavacas, A. Lauchner, V. S. Marangoni, C. J. DeSantis, P. Nordlander, and N. J. Halas, J. Phys. Chem. Lett. **8**, 2060 (2017).

[11] M. T. Sheldon, J. Van de Groep, A. M. Brown, A. Polman, and H. A. Atwater, Science **346**, 828 (2014).

[12] E. Le Ru and P. Etchegoin, *Principles of Surface-Enhanced Raman Spectroscopy: And Related Plasmonic Effects* (Elsevier, Oxford, 2008).

[13] A. Kabashin, P. Evans, S. Pastkovsky, W. Hendren, G. Wurtz, R. Atkinson, R. Pollard, V. Podolskiy, and A. Zayats, Nat. Mater. **8**, 867 (2009).

[14] K. A. Willets and R. P. Van Duyne, Annu. Rev. Phys. Chem. **58**, 267 (2007).

[15] A. M. Gobin, M. H. Lee, N. J. Halas, W. D. James, R. A. Drezek, and J. L. West, Nano Lett. **7**, 1929 (2007).

[16] C. Ayala-Orozco, C. Urban, M. W. Knight, A. S. Urban, O. Neumann, S. W. Bishnoi, S. Mukherjee, A. M. Goodman, H. Charron, T. Mitchell, M. Shea, R. Roy, S. Nanda, R. Schiff, N. J. Halas, and A. Joshi, ACS Nano **8**, 6372 (2014).

[17] M. Muller, V. Kravtsov, A. Paarmann, M. B. Raschke, and R. Ernstorfer, ACS Photonics **3**, 611 (2016).

[18] F. Krausz and M. I. Stockman, Nat. Photonics **8**, 205 (2014).

[19] S. R. Leone, C. W. McCurdy, J. Burgdörfer, L. S. Cederbaum, Z. Chang, N. Dudovich, J. Feist, C. H. Greene, M. Ivanov, R. Kienberger, U. Keller, M. F. Kling, Z.-H. Loh, T. Pfeifer, A. N. Pfeiffer, R. Santra, K. Schafer, A. Stolow, U. Thumm, and M. J. J. Vrakking, Nat. Photonics **8**, 162 (2014).

[20] U. Thumm, Q. Liao, E. M. Bothschafter, F. Süßmann, M. F. Kling, and R. Kienberger, *Fundamentals of photonics and physics*, Vol. 1 (Wiley, New York, 2015) Chap. 13.

[21] R. Kienberger, E. Goulielmakis, M. Uiberacker, A. Baltuska, V. Yakovlev, F. Bammer, A. Scrinzi, T. Westerwalbesloh, U. Kleineberg, U. Heinzmann, M. Drescher, and F. Krausz, Nature **427**, 817 (2004).

[22] E. Saydanzad, J. Li, and U. Thumm, Phys. Rev. A **95**, 053406 (2017).

[23] J. Li, E. Saydanzad, and U. Thumm, Phys. Rev. A **95**, 043423 (2017).

[24] F. Süßmann and M. F. Kling, Phys. Rev. B **84**, 121406 (2011).

[25] B. Förg, J. Schötz, F. Süßmann, M. Foerster, M. Krueger, B. Ahn, W. Okell, K. Wintersperger, S. Zherebtsov, A. Guggenmos, V. Pervak, A. Kessel, S. A. Trushin, A. M. Azzeer, M. I. Stockman, D. Kim, F. Krausz, P. Hommelhoff, and M. F. Kling, Nat. Commun. **7**, 11717 (2016).

[26] J. Schötz, B. Förg, M. Förster, W. A. Okell, M. I. Stockman, F. Krausz, P. Hommelhoff, and M. F. Kling, IEEE J. Sel. Top. Quantum Electron. **23**, 8700111 (2017).

[27] J. Li, E. Saydanzad, and U. Thumm, Phys. Rev. Lett. **120**, 223903 (2018).

[28] J. L. Ellis, D. D. Hickstein, W. Xiong, F. Dollar, B. B. Palm, K. E. Keister, K. M. Dorney, C. Ding, T. Fan, M. B. Wilker, K. J. Schnitzenbaumer, G. Dukovic, J. L. Jimenez, H. C. Kapteyn, and M. M. Murnane, J. Phys. Chem. Lett. **7**, 609 (2016).

[29] F. Süßmann, L. Seiffert, S. Zherebtsov, V. Mondes, J. Stierle, M. Arbeiter, J. Plenge, P. Rupp, C. Peltz, A. Kessel, S. Trushin, B. Ahn, D. Kim, C. Graf, E. Ruhl, M. Kling, and T. Fennel, Nat. Commun. **6**, 7944 (2015).

[30] L. Seiffert, Q. Liu, S. Zherebtsov, A. Trabattoni, P. Rupp, M. Castrovilli, M. Galli, F. Süßmann, K. Wintersperger, J. Stierle, G. Sansone, L. Poletto, F. Frassetto, I. Halfpap, V. Mondes, C. Graf, E. Rühl, F. Krausz, M. Nisoli, T. Fennel, F. Calegari, and M. F. Kling, Nat. Phys. **13**, 766 (2017).

[31] J. Powell, S. Robatjazi, A. Vajdu, V. Makhija, J. Stierle, X. Li, Y. Malakar, W. L. Pearson, C. Sorensen, M. F. Kling, and A. Rudenko, in *CLEO: QELS_Fundamental Science* (Optical Society of America, 2016) pp. FTh4M–3.

[32] A. M. Summers, A. S. Ramm, G. Paneru, M. F. Kling, B. N. Flanders, and C. A. Trallero-Herrero, Opt. Express **22**, 4235 (2014).

[33] J. D. Jackson, *Classical electrodynamics, 3rd ed.* (Wiley, New York, 1999).

[34] G. Mie, Ann. Phys. (Berlin) **330**, 377 (1908).

[35] H. Kuwata, H. Tamaru, K. Esumi, and K. Miyano, Appl. Phys. Lett. **83**, 4625 (2003).